Journal of Catalysis 447 (2025) 116151

Contents lists available at ScienceDirect

Journal of Catalysis

journal homepage: www.elsevier.com/locate/jcat

Research article

# Effect of elastic strains on the electrocatalytic activity of Au thin films for the hydrogen evolution reaction

J. Redondo [a,b], J. Subbian [a], M.A. Monclús [a], A. Pendashteh [a], D. Pérez [b,d], M. Mehdi [a], J. Ruiz-Hervías [b,d], J.M. Molina Aldareguia [a,c], J. LLorca [a,b,*]

[a] IMDEA Materials Institute, C/Eric Kandel 2, 28906 Getafe, Madrid, Spain
[b] Department of Materials Science, Polytechnic University of Madrid/Universidad Politécnica de Madrid, E. T. S. de Ingenieros de Caminos, 28040 Madrid, Spain
[c] Department of Mechanical Engineering Polytechnic University of Madrid/Universidad Politécnica de Madrid, C/Jose Gutierrez Abascal 2, 28006 Madrid, Spain
[d] Research Center for Structural Materials (CIME), Polytechnic University of Madrid/Universidad Politécnica de Madrid 28040 Madrid, Spain

ARTICLE INFO

*Keywords:*
Hydrogen evolution reaction
Elastic strain engineering
Elastic strains
Shape memory alloys
Au

ABSTRACT

Platinum-group metals are currently the most efficient catalysts for hydrogen evolution reaction (HER), however their high cost and scarcity urge introduction and development of affordable alternatives. Herein, the effect of elastic strains on gold (Au) thin films is investigated to tune and enhance their catalytic activity towards HER. Tensile and compressive strains are introduced into Au films deposited via magnetron sputtering onto nitinol substrates using one-way shape memory effect of the alloy. The generated elastic strains are measured by X-ray diffraction, revealing maximum ~ 0.43 % tension and ~ 0.25 % compression. Electrochemical tests demonstrate that applying tensile strains to the Au thin film increases the HER catalytic activity, e.g., by reducing the overpotential at 50 mA/cm$^2$ by 24 %. On the contrary, compressive strains decrease the catalytic activity, resulting in an increased overpotential of 32 %. Such effect is further confirmed from the kinetics study through Tafel analysis and charge transfer resistance measurements. Accordingly, this study not only results in Au samples with improved HER activity but also paves the path towards better understanding and application of elastic strain engineering for metals with enhanced catalytic activity for sustainable hydrogen production.

## 1. Introduction

The hydrogen economy is one of the most promising strategies to spread the use of clean energies in the world. Within this framework, hydrogen is generated by water splitting through a catalytic process involving the hydrogen evolution reaction (HER) in the cathode and the oxygen evolution reaction in the anode. Both reactions require high overpotentials or temperatures to attain substantial rates [1,2] and efficient catalysts are necessary to overcome this limitation. In particular, the HER is a classic example of a two-electron transfer reaction through the Volmer-Heyrovsky or Volmer-Tafel mechanisms [3], with hindered kinetics by hydrogen adsorption on the surface: the adsorption process (Volmer) limits the kinetics if hydrogen binds weakly on the catalyst surface, while desorption (Heyrovsky/Tafel) is the limiting process otherwise.

Typically, Pt –and other Pt-group metal compounds- are used as catalysts for the HER in acidic environments due to its efficiency, stability, and selectivity, but its availability and price stand as a limiting factor from the industrial viewpoint [4–7]. Thus, the search for cheaper and more affordable catalysts that can compete with Pt-group metals is an active area of research [8,9].

Application of elastic strains has been widely recognized as an interesting strategy to improve the activity of heterogeneous catalysts [10]. In general, the effect of elastic deformations on the physical and chemical properties of materials becomes relevant when elastic strains equal to or greater than 1 % are reached [11,12]. These levels of elastic deformation cannot be reached in tension or shear in bulk solids because defects –such as dislocations or cracks- develop at lower elastic strains. However, they can be achieved in nanomaterials (nanowires, two-dimensional materials), thin foils or bulk nanostructured materials [13,14]. These deformations associated to the microstructure of the material (e.g. epitaxial deformations in a thin foil) or applied from external sources. Thus, the electronic, optical, magnetic, catalytic, etc. properties of solids can be modified by systematically varying the 6 components of the elastic strain tensor. This strategy opens many opportunities to develop materials with optimized functional properties for

* Corresponding author.
*E-mail addresses:* javier.llorca@upm.es, javier.llorca@imdea.org (J. LLorca).

https://doi.org/10.1016/j.jcat.2025.116151
Received 24 December 2024; Received in revised form 7 March 2025; Accepted 15 April 2025
Available online 16 April 2025

specific applications.

The contribution of elastic strains to improve catalytic properties of Pt-based nanoparticles for the HER has been recognized [1] and these results are supported by first principles calculations that show the effect of elastic strains on the adsorption of hydrogen on different metallic surfaces [15]. In fact, density functional theory calculations of the adsorption energy of H on 8 face-centered cubic (Rh, Ir, Ni, Cu, Pt, Au, Pd, Ag) and 3 hexagonal closed packed (Cd, Zn, Co) transition metal surfaces were carried as a function of tensile, compressive, and shear strains. This information was used to calculate volcano plots of the catalytic activity for the HER following the strategy developed by Nørskov et al. [16], in which the free energy of every step in the HER mechanism is calculated from the adsorption energies of the different species involved [17,18]. The volcano plots for the HER in the absence of strain were in good agreement with the experimental data in the literature, validating the theoretical model. Moreover, it was predicted that compressive strains increased the catalytic activity of metals on the ascending branch of the volcanos (Pt, Pd, Rh, Ni, and Ir) because they decreased the energy barrier for H* desorption, which is the limiting step. On the contrary, tensile strains improved the activity of metals in the descending branch of the volcano, as they decreased the energy barrier for H adsorption (Au and Ag). The largest improvements in activity were found in Au, which had a large sensitivity of the H adsorption energy to elastic strains. Smetanin M. et al. [19] observed the change in the electrical response of an Au electrode to tensile strains but did not investigate the HER.

Elastic deformations can be introduced using catalysts in the form of particles with a diameter of less than 10 nm [20] and/or by adding elements in solid solution whose atomic radius is much less than or greater than the radius of the host atoms [21–23]. Moreover, epitaxial growth can also be used to introduce elastic strains in thin films [24]. However, the sign and magnitude of the elastic strains that can be introduced through these strategies is often limited and does not allow to explore a wide range of strains and materials.

A more versatile strategy to introduce tensile or compressive elastic strains on thin films is presented in this investigation. It is based on the deposition of the catalytic thin film by magnetron sputtering on a NiTi alloy substrate, to take advantage of its shape memory effect [25–27]. With this strategy, the Au thin film is deposited on a nitinol substrate that has been previously curved by four-point bending from its initially flat shape. After deposition, heating induces the shape memory effect in the substrate, which results in it recovering its initial flat shape and straining the thin film in the process [28]. Tensile or compressive strains can be induced on the thin film, depending on whether it is deposited on the concave or convex surface of the substrate, respectively. Afterwards, the elastic strains induced in the film can be measured by X-ray diffraction [29–31] while the catalytic activity is obtained using standard electromechanical tests. This strategy allows us to explore experimentally the effect of elastic strains on the catalytic activity of thin films manufactured by magnetron sputtering.

## 2. Experimental section

### 2.1. Substrate preparation

NiTi substrates were acquired from Baoji Seabird Metal Material Co. Ltd. in the form of 50 mm × 10 mm × 1.5 mm slabs with a nominal composition of 50 at. % Ti – 50 at. % Ni. The specimens were ground and polished to a mirror-like surface, achieving an average surface roughness of 40 nm. The substrates then were deformed in the martensitic state at room temperature using a 4-point bending set-up. Inner supports were placed 10 mm away from each other, so the maximum strain can be applied to an area of ≈100 $mm^2$ (Fig. 1a). The outer supports were placed 40 mm apart. A force of 270 N was applied to the substrates, leading to a deflection of 10 mm. The positive (negative) strain, $\varepsilon$, on the lower (upper) surface of the slab is given by the equation [32]:

$$\varepsilon = \frac{6dt}{L^2} \tag{1}$$

where $d$ is the deflection, $t$ is the thickness of the NiTi substrate, and $L$ represents distance between the outer supports (Fig. 1b). For the actual dimensions and the deflection applied, the maximum strain was 5.6 % (positive on the lower surface and negative in the upper one).

### 2.2. Au thin film deposition

Polycrystalline Au thin films were deposited on either the concave or the convex sides of the NiTi substrates at room temperature by direct current magnetron sputtering. The sputtering chamber was evacuated to a base pressure of $6x10^{-6}$ mbar. Prior to Au deposition, a thin Cr bonding layer was deposited onto the NiTi substrate to improve the adhesion of the Au thin film onto the substrate. The Cr bonding layer was deposited at a power of 10 W over 1 min, resulting in a 6–7 nm-thick layer of Cr. The amorphous nature of the Cr bonding layer is supported by the absence of diffraction peaks of Cr in the X-Ray diffractograms. Afterwards, Au thin film deposition was carried out from a 99.99 %-pure Au

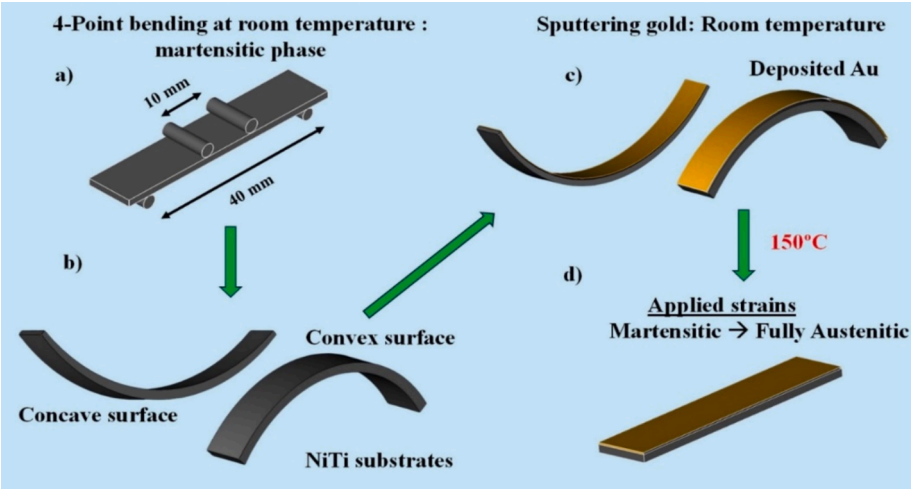


**Fig. 1.** Schematic representation for the procedure to apply elastic strains on Au thin films using shape memory effect of NiTi. (a) 4-point bending of martensitic NiTi substrates. (b) Bent NiTi substrates. (c) Sputtered gold on concave/convex surface of NiTi substrates. (d) Phase change of NiTi substrate heated on a hot plate with Au on top of it.

(Photon Export S.L) target using an Ar working pressure of 2.7x10-3 mbar, at 10 W. The goal was to obtain an Au film of ≈ 100 nm in thickness. A deposition rate of ≈0.083 nm/s was estimated according to the Au thin film thickness obtained after 20 min of deposition.

### 2.3. Introduction of elastic strains

Elastic strains in the Au thin films were introduced using the one-way shape memory effect (OWSME) of NiTi. After deposition (Fig. 1c), the Au thin film/substrate was heated up to 150 °C to trigger the phase transformation in the NiTi substrate from the martensitic to the austenitic phase. As a result, the curved NiTi substrate recovered the initial flat shape, which deforms the Au thin film with respect to the as-deposited state. For those cases in which the Au was deposited onto the concave side of the curve substrate, shape recovery deforms the thin film in tension, while those deposited on the convex shape result in compressive deformations (Fig. 1d). Based on equation (1), the maximum deformation imposed on the Au films using this method would be 5.6 %. However, the total elastic strain introduced in the thin films might be lower due to plastic relaxation effects, film debonding and/or cracking, and it must be determined by XRD as shown below.

### 2.4. Material characterization

An X-raybot (MRX Rays) X-ray diffractometer was employed to measure the elastic strains in the as-deposited and strained gold thin films, using Bragg's law ($2d\sin\theta = \lambda$), where $d$ is the interplanar spacing, $2\theta$ the diffraction angle (between the incident and diffracted beam), and $\lambda$ the X-ray wavelength. K-alpha radiation from a Cr source was used ($\lambda = 0.2291$ nm), resulting in a diffraction peak around $2\theta = 153^\circ$ for the Au (2 2 2) planes, with $\chi = 0^\circ$ and $\varphi = 90^\circ$, where $\chi$ is the tilt angle, which defines the inclination of the sample surface relative to the plane that is perpendicular to the incident beam; and $\phi$, the azimuthal angle, defines the in-plane rotation of the sample with respect to the incident beam. The diffraction measurements were focused specifically on grains that had the (222) planes parallel to the film surface, due to the strong texture of the thin films. This orientation was chosen because the (222) planes in face-centered cubic (FCC) materials, such as Au, stand for a high-symmetry direction that is sensitive to strain, making easier to quantify accurately elastic deformations. The measurement range of $2\theta$ employed was between 141.9° and 170°, which covers the expected range for the diffraction peak of the (222) planes under different strain states. The penetration depth was determined based on the diffraction angle and the linear attenuation coefficient, obtaining a value of 0.42 μm. The mass attenuation coefficient for Au was calculated using the data from National Institute of Standards and Technology (NIST), interpolating the tabulated values for the photon energy corresponding to the employed wavelength. Finally, a collimator of 2 mm in diameter was used, giving a radiated spot size of 2.5 mm. The XRD measurements were performed inside the 10 $mm^2$ area where the elastic strains were maximum (Fig. 1).

An Empyrean Diffractometer (Malvern Panalytical LTD) was employed to assess the phase characterization of the NiTi substrates. Bragg-Brentano measurement was employed in a flat stage, from 20° to 85° of $2\theta$ at scan speed of 0.0514 °/s and Cu source.

A TA Instruments Q200 Differential Scanning Calorimeter (DSC) was used to conduct DSC measurements of the NiTi within a temperature range of −90 °C to 140 °C under a nitrogen atmosphere. Both heating and cooling rates were maintained at 10 °C/min. The transformation temperatures—namely, the martensite start (Ms), martensite finish (Mf), austenite start (As), and austenite finish (Af)—were determined from the resulting curves using the tangent method.

The topography of the surface was analyzed using a XE-150 Parks system AFM. AFM imaging of the samples was performed in non-contact mode using a scan area of 1x1 $\mu m^2$ and a resolution of 1024 × 1024 pixels.

The microstructure of the films was investigated by Transmission Electron Microscopy (TEM) using a Thermofischer FEI F200X and by Scanning Electron Microscopy (SEM) using a ThermoFisher Helios Nanolab 600i instrument. Thin lamella of approximately 100 nm in thickness and perpendicular to the cross-section were prepared by the lift-out method using the focused Ga ions of the dual beam Helios Nanolab instrument operated at 30 kV. The final polishing step with Ga ions was performed at 5 kV accelerating voltage and 41 pA ion-current. The average grain size was measured using the ImageJ software with the line intercept method.

### 2.5. Electrochemical measurements

The electrocatalytic activity of the samples for the HER was probed in a three-electrode configuration using the Au thin film/NiTi sample as the working electrode (WE), Ag/AgCl reference electrode (RE), And Pt mesh as counter electrode (CE, BASInc. MW-4132), with an area of 875 $mm^2$, in a 0.5 M $H_2SO_4$ electrolyte. The exposed area of the working electrode was limited to 50 $mm^2$ using a Kapton mask, and NiTi substrate was completely covered to prevent any contact with the electrolyte. All electrochemical measurements were conducted at 25 °C in a double-walled glass vessel and water circulator. The electrochemical experiments were carried out using a BioLogic VSP-300 potentiostat. The potentials were reported against reversible hydrogen electrode (RHE). Prior to any activity measurement, the surface of the catalyst was activated and stabilized by conducting 40 cyclic voltammograms (CV) in a potential range of 0.510 and −0.010 V (vs. RHE) at a scan rate of 20 mV/s. Afterwards, Linear Sweep Voltammetry (LSV) was performed at a scan rate of 1 mV/s between −0.010 V and −0.810 V. The voltage loss was corrected by the ex-situ IR-compensation method. This voltage was subtracted with the voltage drop ($V_{drop}$) calculated from the resistance ($R_s$) obtained in the Electrochemical Impedance Spectroscopy (EIS) under the high frequency region, following the relation: $V_{corrected} = V_{applied} - V_{drop}$, where $V_{drop} = I \cdot R_s$. The IR-correction was performed before every LSV to ensure reproducibility and accuracy of the measured overpotentials. Electrochemical Impedance Spectroscopy (EIS) data were collected under low HER region over a frequency range of 1 MHz to 0.010 Hz.

## 3. Results and discussion

### 3.1. Microstructural analysis of NiTi substrates

The phase transition temperatures were determined by means of differential scanning calorimetry (Fig. 2). To this end, the tangent line intercept method was used to calculate the transformation temperatures. It shows that Ms temperature is 60 °C, the Mf temperature is 21 °C, the As at 50 °C, and the Af at 80 °C. This indicates that the stable phase of the nitinol substrate at room temperature was martensite (B19′), also confirmed by XRD in Fig. 3. Small peaks of $TiO_2$ were found in the diffractogram, which are related to the oxidation NiTi during fabrication. A small amount of retained austenite (≈ 5 %) is present in the substrate at room temperature. According to the transformation temperatures in Fig. 2, room temperature deformation of the nitinol substrate should occur by detwinning of the martensitic phase and shape can be recovered by inducing the phase transformation to austenite upon heating above Af.

### 3.2. Microstructural analysis of Au thin films

The microstructure of the unstrained (pristine) Au thin film was analyzed by TEM. A bright-field TEM image of the cross-section of the Au thin film is shown in Fig. 4a. The thicknesses of the Au thin film and the Cr bonding layer were ≈100 nm and ≈ 7 nm, respectively. The Cr bonding layer was amorphous and provided a good adhesion with the NiTi substrate. The thin film was polycrystalline with columnar grains

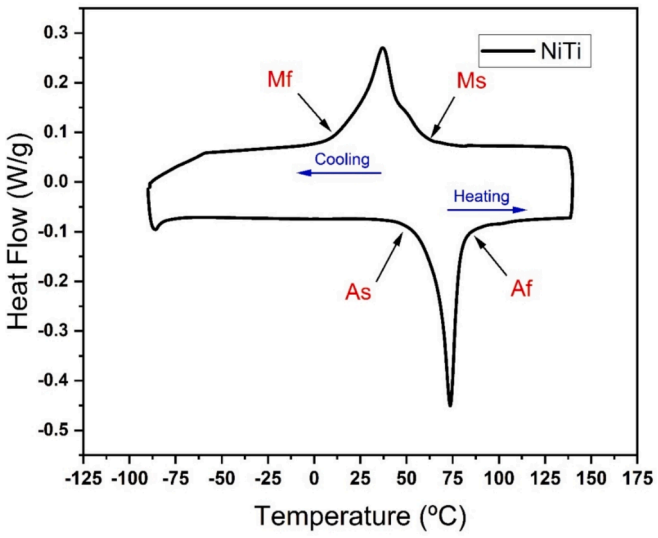


**Fig. 2.** Differential scanning calorimetry test of NiTi substrate. The main transformation temperatures are indicated in the figure.

that grow with a [111] preferred orientation, as shown in the high-resolution transmission electron microscopy (HRTEM) image of Fig. 4b and its corresponding Fast Fourier Transform (FFT) pattern. Fig. 4c shows a magnified HRTEM image close to the surface of the film, which shows lattice fringes whose spacing d = 0.231 nm, is consistent with the fundamental reflection of the Au (1 1 1) plane [33].

The morphological aspect of the Au thin film surface is probed via SEM and the corresponding micrographs are shown for the unstrained sample (Fig. 5a), strained in compression (Fig. 5b) and strained in tension (Fig. 5c). A homogeneous surface with uniform equiaxed grains can be observed in all cases. There are not major differences in the morphology of the films. A few pores and some microcracks can be observed, especially in the strained films (Fig. 5b and c). The average grain size was measured using ImageJ software with the line intercept method. The grain size distribution in the Au film was in the range 23 nm to 35 nm. The average roughness measured by AFM was very similar in all cases: 48 ± 6 nm for the unstrained thin-film (Fig. 5d), 47 ± 7 nm for the film strained in compression (Fig. 5e) and 43 ± 6 nm for the film strained in tension (Fig. 5f).

### 3.3. Measurements of elastic strains

X-ray diffraction (XRD) was employed to measure the elastic strains on the thin films. K-alpha radiation from Cr, which provides a shorter X-ray wavelength, was selected for its ability to produce higher-diffraction angles, thereby optimizing the strain sensitivity and reducing the experimental error. Fig. 6 shows the experimental set-up used.

The elastic strains were determined from the interplanar spacing of the Au (222) planes, parallel to the film surface, determined from the diffraction peak position using Bragg's law. The (222) peak shifts observed in the strained thin films with respect to the as deposited state are seen in Fig. 7. The film strained in tension displays a shift of the (222) peak to higher diffraction angles, indicating a reduction in their interplanar spacing, which is expected due to the Poisson effect. The contrary was seen in compression. Two hypotheses were made to estimate the elastic strains. The first hypothesis neglects any elastic strain present in the thin film in the as-deposited condition, considering this as the reference unstrained state. The second one assumes that the shape recovery from the bent to the flat substrate introduces a uniaxial strain in the thin film, which is reasonable considering that the curvature was introduced by four-point bending.

If $d_{exp}$ is the (002) lattice spacing measured after shape recovery and d0 is the lattice spacing in the as-deposited unstrained state, the out-of-plane strain $\varepsilon\perp$, that is the strain along the (222) direction, or perpendicular to the surface of the Au thin film, is given by:

$$\varepsilon_{\perp} = \frac{d_{exp} - d_0}{d_0} \quad (2)$$

The in-plane elastic strain in the direction parallel to the longest dimension of thin film, that is the one along all the surface of the Au thin film and the strain that effects on the catalytic activity of it, is then given

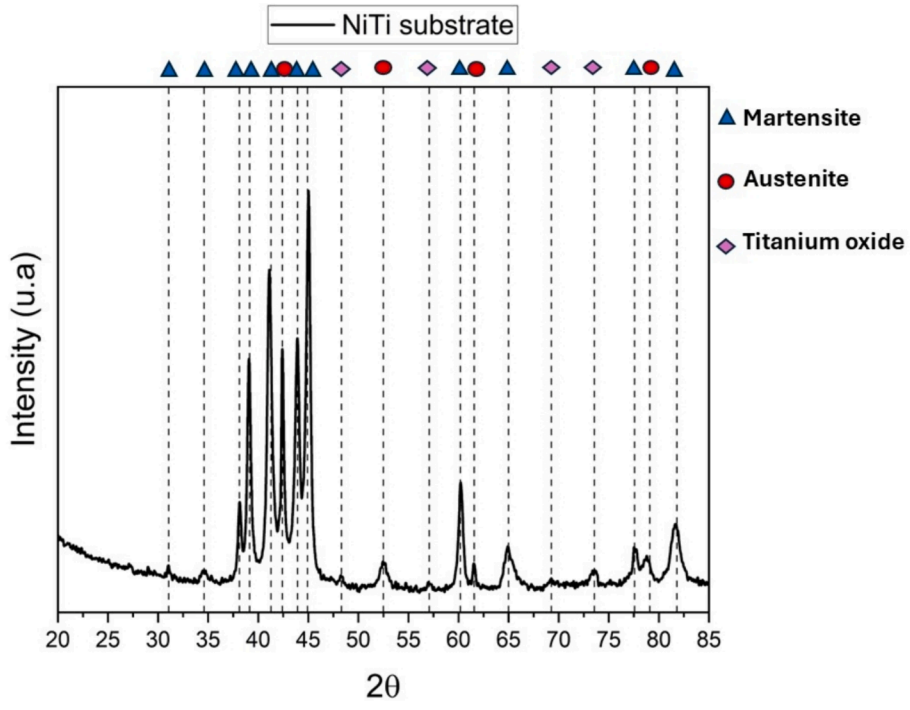


**Fig. 3.** X-ray diffraction pattern in Bragg-Brentano mode of NiTi substrate with Cu source at room temperature.

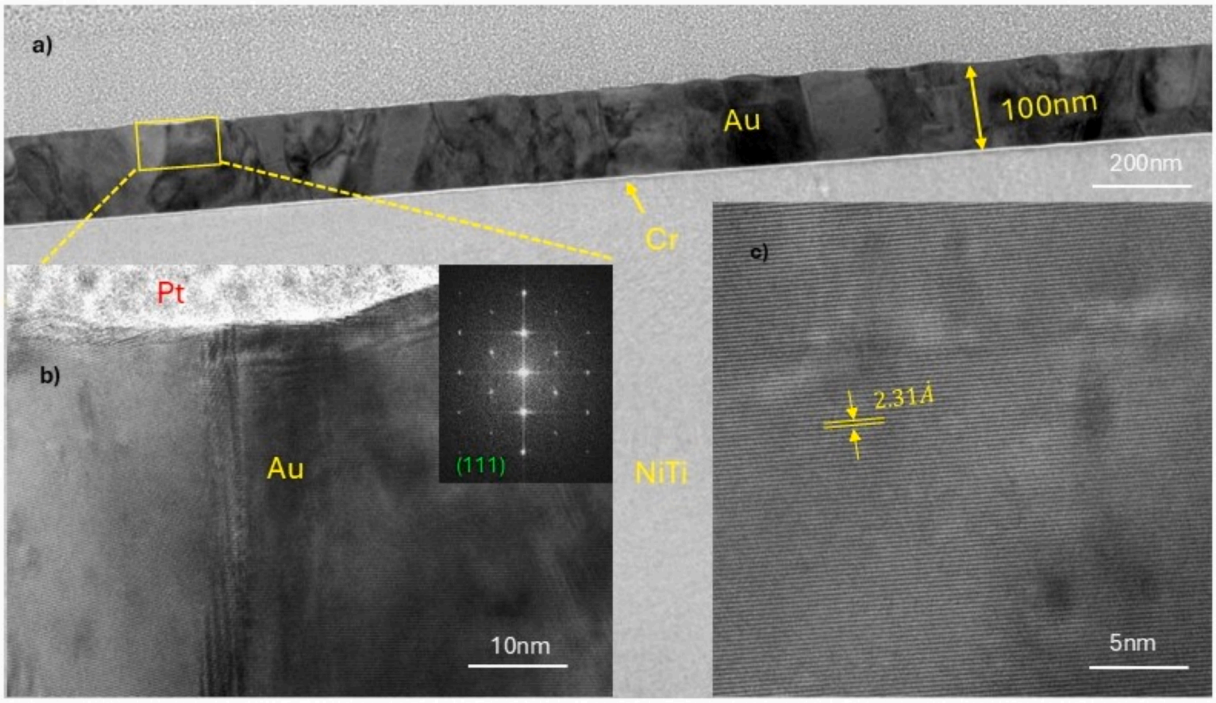


**Fig. 4.** (a) Bright field tem image of the cross-section of the NiTi/Cr/Au sample. (b) and (c) HRTEM images of the selected Au grain.

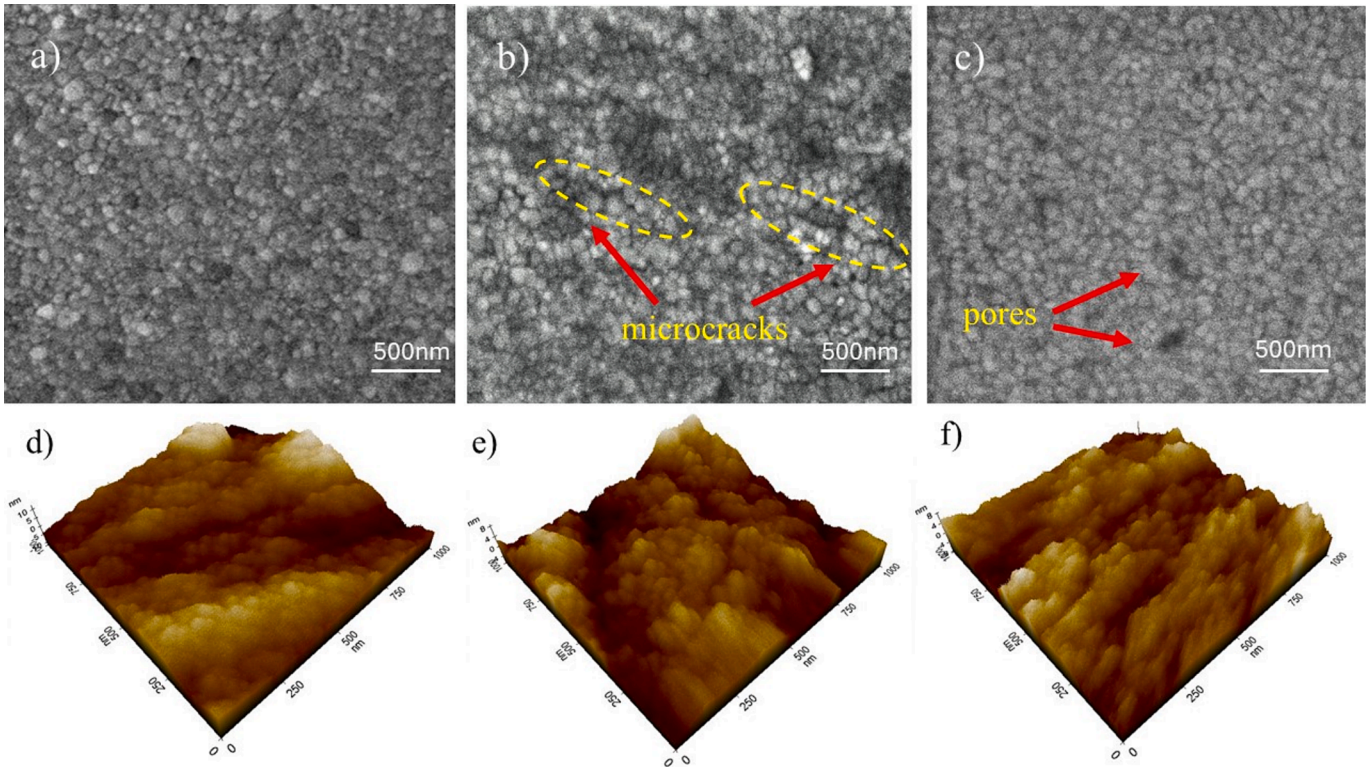


**Fig. 5.** SEM images of the surface of the Au thin films. (a) Unstrained, (b) deformed in compression and (c) deformed in tension and corresponding AFM images for (d) unstrained, (e) deformed in compression and (f) deformed in tension.

from:

$$\varepsilon\| = -\frac{\varepsilon_{\perp}}{\nu} \tag{3}$$

where $\nu = 0.42$ [34] is the Poisson's ratio of Au along the (111) direction.

The estimated elastic strains in the strained Au films were 0.43 % in tension and 0.27 % in compression, as shown in Table 1. The actual elastic strains were much lower than the total strain of 5.6 % estimated if the entire substrate shape recovery was transferred to the films. These

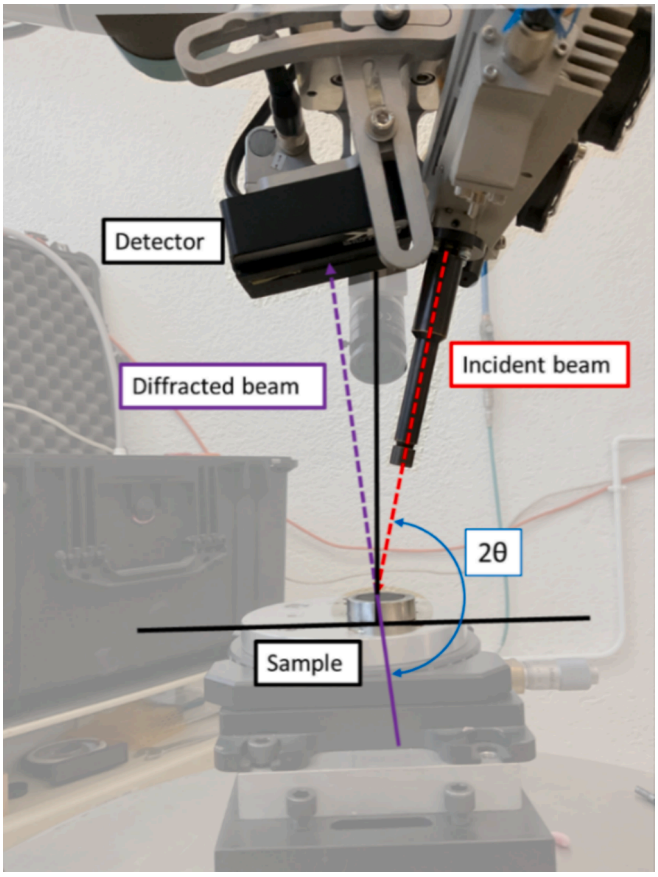


**Fig. 6.** X-Ray diffraction set up used to measure elastic strains.

differences can be associated to relaxation effects, such as plastic deformation, debonding or cracking of the Au film. The cross-sectional analysis of the films did not reveal any decohesion at either the NiTi/Cr or the Au/Cr interface, but some cracks and pores could be seen in the strained Au thin films in Fig. 5a and 5b. The elastic strains obtained are not far from the theoretical maximum elastic strain that a 100 nm thick Au thin film can withstand, which have been estimated to be of the order of 1 %-1.5 % in tension and 0.5 % in compression in other studies [33,34].

### 3.4. Strain effect on HER activity

The surface of Au films, unstrained (pristine) and subjected to compressive and tensile strains, was first stabilized by conducting 40 CV cycles at 20 mV/s. The current density is plotted as a function of the IR-corrected potential in Fig. 8 during consecutive cycles for the three films. As it is seen for all the samples, the current density increases gradually over cycling. The most significant gains in current are found in the initial cycles, indicating improved activity as a result of surface electrochemical activation.

Afterwards, the HER electrocatalytic activity of the films was probed using different electrochemical techniques. Fig. 9(a) shows the LSV curves after IR-correction, demonstrating superior electrocatalytic activity of the tensile sample with the smallest overpotential, with 175 mV vs. RHE at 50 mA/cm$^2$. On the contrary, the compressive sample exhibited the highest overpotential, with 305 mV under the same

**Table 1**
Peak position for Au (222) peak, corresponding $d_{222}$ spacing and calculated elastic strain of unstrained and strained Au thin films.

| Sample | $2\theta$ | $d_{222}$(nm) | $\varepsilon\|$(%) |
|---|---|---|---|
| Unstrained | 152.81 ± 0.042 | 1.1780 ± 0.005 | 0 |
| Tensile strained | 153.67 ± 0.034 | 1.1759 ± 0.008 | 0.43 |
| Compressive strained | 152.29 ± 0.029 | 1.1793 ± 0.007 | −0.27 |

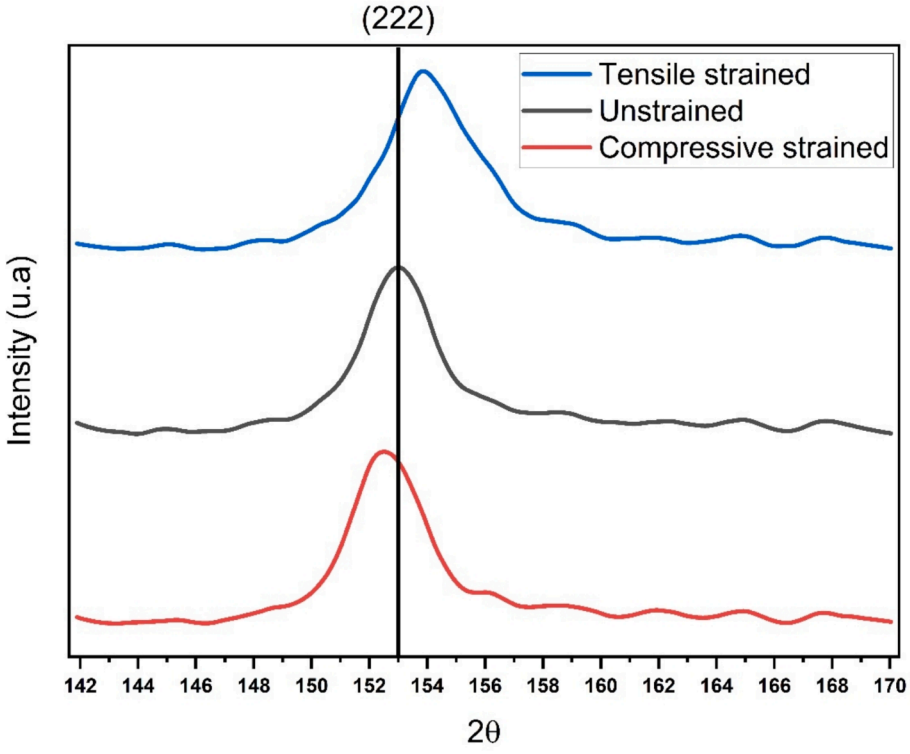


**Fig. 7.** Peak position for Au (222) peak.

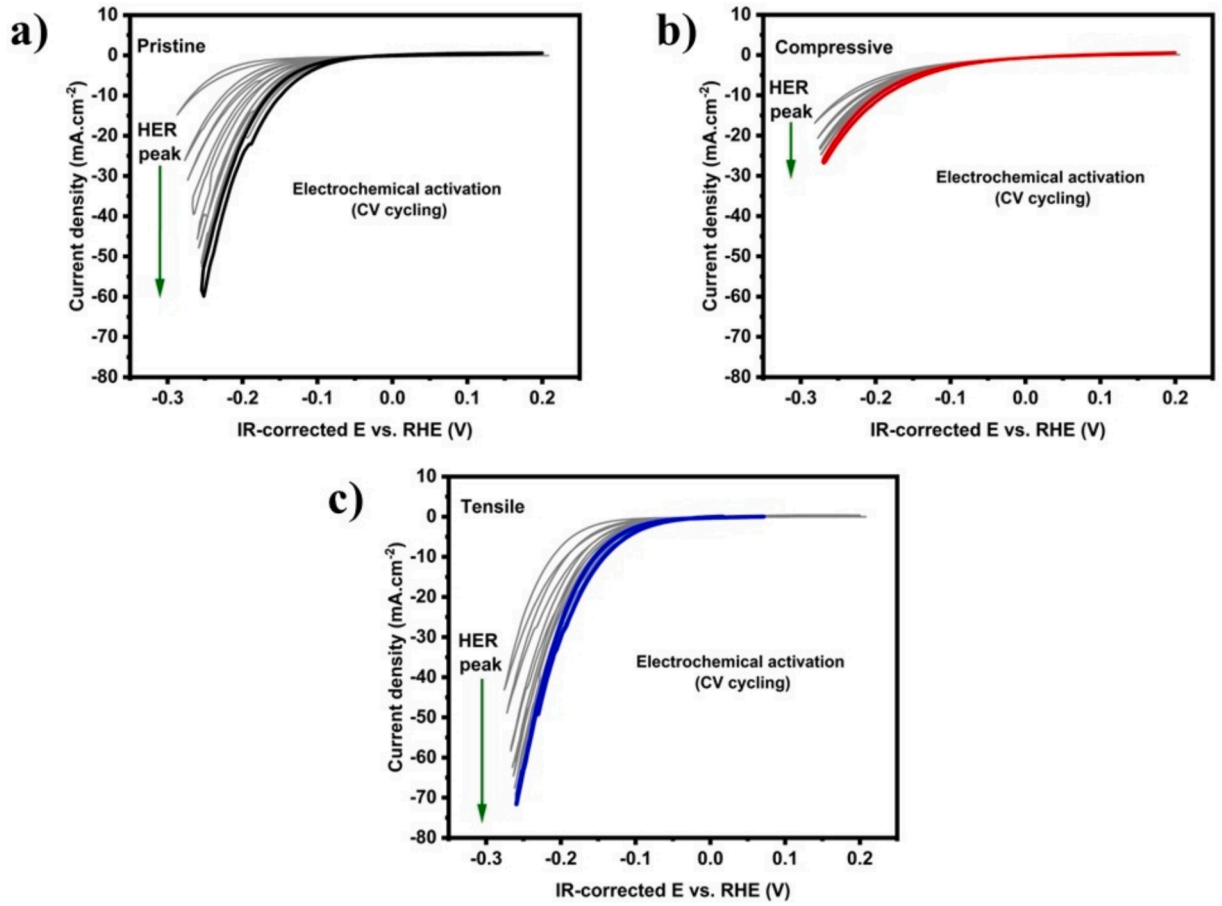


**Fig. 8.** Electrochemical activation of Au thin films in 0.5 $H_2SO_4$ acidic solution at 25 °C during 40 CV cycles (0.510 to −0.010 V vs. RHE, 20 mV/s). (a) Unstrained. (b) Under compression. (c) Under tension. CVs are shown from top to bottom at 5-cycle intervals, displaying cycles 1, 5, 10, 15, 20, 25, 30, 35, and 40.

conditions, and inferior to that of the pristine one, with 230 mV. The corresponding Tafel plots are reported in Fig. 9(b). They reveal that tensile strains lead to the smallest Tafel slope, 84 mV/dec, followed by the unstrained catalyst, 93 mV/dec, and the sampled subjected to compressive strains, that presents the highest slope, 156 mV/dec. This observation demonstrates that the HER kinetics are faster on the tensile thin films. Furthermore, these Tafel slopes suggest that the Volmer step ($H+ + e- \rightarrow H^*$) is the rate-determining step for all three electrodes, where a proton is adsorbed onto the electrode surface to form an adsorbed hydrogen atom (H*), in agreement with the theoretical analysis [35].

The boosted HER electrocatalytic activity of Au under tensile strain was further supported by impedance measurements at HER dominant potential (−0.3 V vs. RHE), shown in Fig. 9(c). As is seen, the Nyquist plot for all three electrodes has the shape of a suppressed semi-circle, with the tensile electrode showing the smallest diameter and overall impedance, corresponding to the best catalytic performance. The experimental data were fitted to a Randel equivalent circuit, including solution resistance ($R_s$) double-layer capacitance ($C_{dl}$) representing charge storage at the electrode–electrolyte interface, and charge transfer resistance ($R_{ct}$), which directly indicates the surface's conductivity toward hydrogen species adsorption. Being a key indicator of catalytic activity, estimated $R_{ct}$ through fitting is shown in Fig. 9(d). The tensile electrode exhibited the lowest $R_{ct}$ value, confirming that its surface is the most active towards HER among all the samples tested here.

The resulting catalytic performance showed a clear dependence on the nature of the strain, with tensile strain significantly enhancing activity and compressive strain having the opposite effect. These results validate the theoretical predictions made by Martínez-Alonso et al. [19] that tensile strains reduce the energy barriers for hydrogen adsorption, a critical step in HER. Beyond the practical implications, this work bridges experimental and computational studies in the field of strain-engineered catalysis, offering a pathway to tailor the catalytic properties of noble metals through controlled deformation. The agreement between our experimental findings and computational predictions strengthens the case for integrating strain-engineering strategies into catalyst design frameworks, particularly for applications in renewable energy technologies such as water splitting and hydrogen production.

The use of XRD to confirm the application of elastic strain and the systematic evaluation of catalytic performance through LSV, Tafel plots and charge transfer resistance analysis provided robust experimental evidence for the relationship between strain and HER activity. The observed 24 % improvement in activity under tensile strain highlights the feasibility of using elastic deformation to tune the electronic and chemical properties of Au thin films, while the 32 % reduction in activity under compressive strain underscores the importance of strain type and magnitude in designing optimized electrocatalysts.

Future work could expand on this foundation by exploring other catalytic systems and investigating the long-term stability of strained configurations under operational conditions. The incorporation of additional analytical techniques, such as in situ stress measurements and advanced surface characterization methods, could provide deeper insights into the mechanistic interplay between strain and catalytic activity. The effect of high intrinsic strains induced by epitaxial growth on thin films deposited by molecular beam epitaxy on the catalytic activity is another interesting area of research. This technique can introduce high elastic strains in the thin film, as shown in [36]; however, it involves complex conditions such as ultra-high vacuum and appropriate

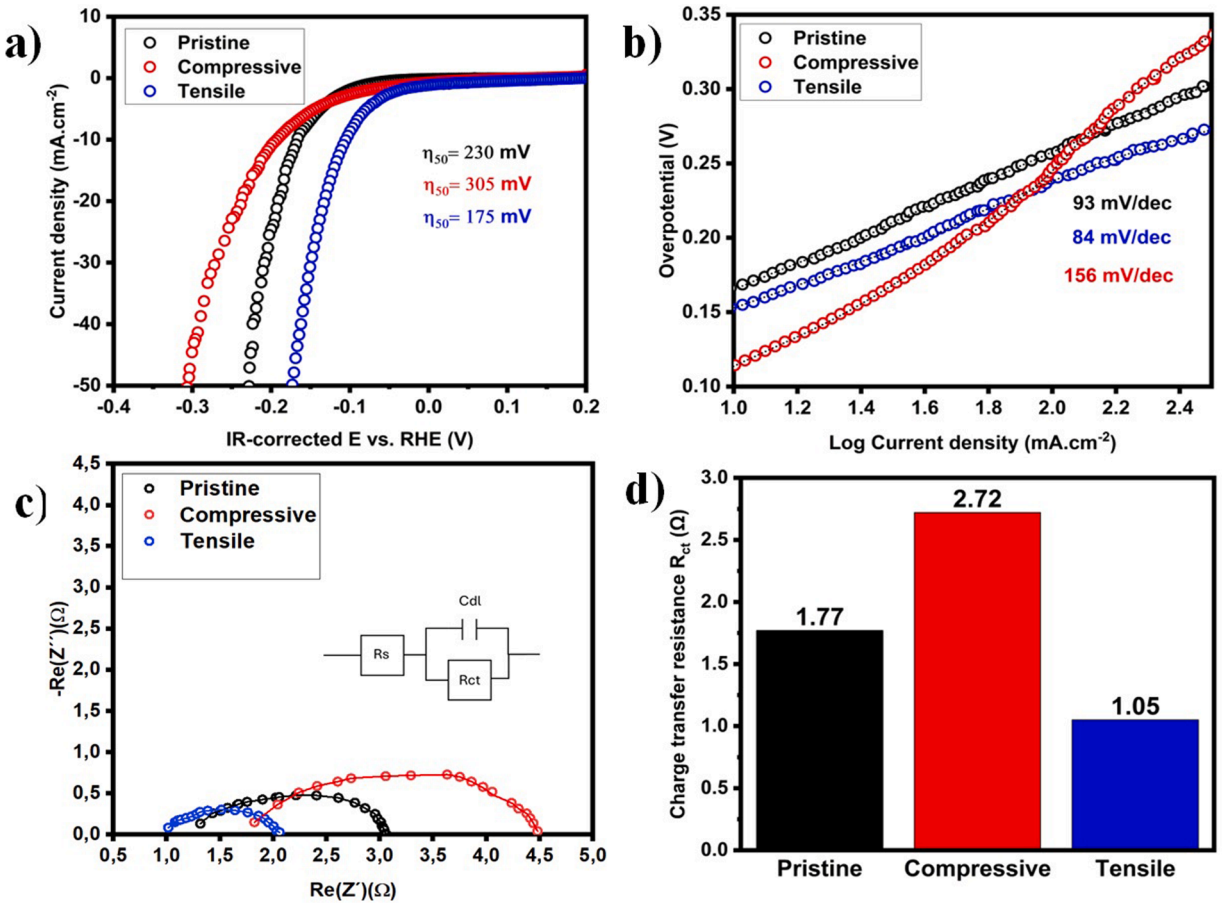


**Fig. 9.** HER catalytic activity performance of pristine, compressive, and tensile Au electrodes in 0.5 M $H_2SO_4$ electrolyte at 25 °C after electrochemical activation: (a) IR-corrected LSV, (b) corresponding Tafel slopes, (c) EIS at −0.3 V vs. RHE with embedded equivalent circuit used for fitting and the fitting associated to it (solid lines), and (d) the estimated charge transfer resistance ($R_{ct}$) for each sample.

selection of a substrate with the proper lattice parameter. Overall, this study underscores the transformative potential of strain-engineering in advancing the performance of next-generation electrocatalysts.

## 4. Conclusions

A shape memory alloy (NiTi) was used as a substrate to introduce elastic strains in Au thin films to modify their catalytic activity for the HER. To this end, the NiTi substrates were deformed by four-point bending, the Au thin was deposited by magnetron sputtering on the convex or concave surfaces of the substrate and elastic strains were incorporated when the substrate recovered the initial shape as a result of the heating that induced the shape recovery. The magnitude of the tensile (0.43 %) and compressive (0.27 %) elastic strains was measured by XRD analysis. It was found that the tensile strains in the Au thin film increased the catalytic activity of Au for the HER by reducing by 24 % the overpotential at 50 mA/cm$^2$. On the contrary, compressive strain decreased the catalytic activity by increasing the overpotential by 32 % at the same current density. This behavior was further confirmed from the kinetics of the reaction according to the Tafel plots and the charge transfer resistance.

The results confirm that the electrocatalytic activity of Au thin films towards HER can be modulated by applying elastic strains and that tensile strains can boost Au performance. These experimental findings align well with previous computational predictions, demonstrating that tensile strains lower the energy barriers for hydrogen adsorption in Au.

## CRediT authorship contribution statement

**J. Redondo:** Writing – review & editing, Writing – original draft, Investigation. **J. Subbian:** Writing – review & editing, Writing – original draft, Investigation. **M.A. Monclús:** Writing – review & editing, Methodology, Investigation. **A. Pendashteh:** Writing – review & editing, Methodology. **D. Pérez:** Writing – review & editing, Investigation. **M. Mehdi:** Writing – review & editing, Methodology, Investigation. **J. Ruiz-Hervías:** Writing – review & editing, Methodology. **J.M. Molina Aldareguia:** Writing – review & editing, Supervision, Methodology, Conceptualization. **J. LLorca:** Writing – review & editing, Writing – original draft, Supervision, Methodology, Funding acquisition, Conceptualization.

## Declaration of competing interest

The authors declare that they have no known competing financial interests or personal relationships that could have appeared to influence the work reported in this paper.

## Acknowledgments

This work was supported by the CATbyESE project (TED2021-129497B-I00) funded by Spanish Ministry of Science and Innovation. X-Ray measurements to determine the elastic strain were carried out at the Residual Stress Measurement Laboratory (LMTR) of the Polytechnic University of Madrid. JR also acknowledges the support from the Spanish Ministry of Science and Innovation through the Fellowship

PRE2021-097425.

## Data availability

Data will be made available on request.

## References


[1] Y. Jiao, Y. Zheng, M. Jaroniec, S.Z. Qiao, Design of electrocatalysts for oxygen- and hydrogen-involving energy conversion reactions, Chem. Soc. Rev. 44 (2015) 2060–2086, https://doi.org/10.1039/c4cs00470a.

[2] S. Wang, A. Lu, C.J. Zhong, Hydrogen production from water electrolysis: role of catalysts, Nano Converg. 8 (2021), https://doi.org/10.1186/s40580-021-00254-x.

[3] N.T. Suen, S.F. Hung, Q. Quan, N. Zhang, Y.J. Xu, H.M. Chen, Electrocatalysis for the oxygen evolution reaction: recent development and future perspectives, Chem. Soc. Rev. 46 (2017) 337–365, https://doi.org/10.1039/c6cs00328a.

[4] N. Dubouis, A. Grimaud, The hydrogen evolution reaction: From material to interfacial descriptors, Chem. Sci. 10 (2019) 9165–9181, https://doi.org/10.1039/c9sc03831k.

[5] A. Ursúa, L.M. Gandía, P. Sanchis, Hydrogen production from water electrolysis: current status and future trends, in: Proceedings of the IEEE, vol. 100, Institute of Electrical and Electronics Engineers Inc.; 2012, p. 410–26. DOI: 10.1109/JPROC.2011.2156750.

[6] M. El-Shafie, Hydrogen production by water electrolysis technologies: a review, Results Eng. 20 (2023), https://doi.org/10.1016/j.rineng.2023.101426.

[7] T.B. Ferriday, P.H. Middleton, M.L. Kolhe, Review of the hydrogen evolution reaction—a basic approach, Energies (basel) 14 (2021), https://doi.org/10.3390/en14248535.

[8] E.J. Popczun, C.G. Read, C.W. Roske, N.S. Lewis, R.E. Schaak, Highly active electrocatalysis of the hydrogen evolution reaction by cobalt phosphide nanoparticles, Angew. Chem. – Int. Ed. 53 (2014) 5427–5430, https://doi.org/10.1002/anie.201402646.

[9] M. Shao, Palladium-based electrocatalysts for hydrogen oxidation and oxygen reduction reactions, J. Power Sources 196 (2011) 2433–2444, https://doi.org/10.1016/j.jpowsour.2010.10.093.

[10] M. Mavrikakis, B. Hammer, J.K. Nørskov, Effect of strain on the reactivity of metal surfaces, Phys. Rev. Lett. 81 (1998) 2819–2822, https://doi.org/10.1103/PhysRevLett.81.2819.

[11] J. Li, Z. Shan, E. Ma, Elastic strain engineering for unprecedented materials properties, MRS Bull. 39 (2014) 108–114, https://doi.org/10.1557/mrs.2014.3.

[12] B. Yildiz, Stretching the energy landscape of oxides - Effects on electrocatalysis and diffusion, MRS Bull. 39 (2014) 147–156, https://doi.org/10.1557/mrs.2014.8.

[13] T. Zhu, J. Li, Ultra-strength materials, Prog. Mater. Sci. 55 (2010) 710–757, https://doi.org/10.1016/j.pmatsci.2010.04.001.

[14] J. Llorca, On the quest for the strongest materials, Science 360 (6386) (2018) 364.

[15] I.G. Shuttleworth, Strain engineering of H/transition metal systems, Surf. Sci. 661 (2017) 49–59.

[16] J.K. Nørskov, T. Bligaard, A. Logadottir, J.R. Kitchin, J.G. Chen, S. Pandelov, et al., Trends in the exchange current for hydrogen evolution, J. Electrochem. Soc. 152 (2005) J23, https://doi.org/10.1149/1.1856988.

[17] C. Martínez-Alonso, J. Manuel Guevara-Vela, J. LLorca, The effect of elastic strains on the adsorption energy of H, O, and OH in transition metals, PCCP 23 (2021) 21295–21306, https://doi.org/10.1039/D1CPO3312C.

[18] C. Martínez-Alonso, J.M. Guevara-Vela, J. LLorca, Understanding the effect of mechanical strains on the catalytic activity of transition metals 2022, PCCP 24 (2022) 4832–4842, https://doi.org/10.1039/D1CP05436H.

[19] M. Smetanin, D. Kramer, S. Mohanan, U. Herr, J. Weissmüller, Response of the potential of a gold electrode to elastic strain, PCCP 11 (2009) 9008–9012, https://doi.org/10.1039/b913448d.

[20] P. Moseley, W.A. Curtin, Computational design of strain in core-shell nanoparticles for optimizing catalytic activity, Nano Lett. 15 (2015) 4089–4095, https://doi.org/10.1021/acs.nanolett.5b01154.

[21] B.R. York, Residual stress/strain analysis in thin films by x-ray diffraction, Crit. Rev. Solid State Mater. Sci. 20 (1995) 125–177, https://doi.org/10.1080/10408439508243733.

[22] S.W. Bedell, A. Khakifirooz, D.K. Sadana, Strain scaling for CMOS, MRS Bull. 39 (2014) 131–137, https://doi.org/10.1557/mrs.2014.5.

[23] V.R. Stamenkovic, B.S. Mun, M. Arenz, K.J.J. Mayrhofer, C.A. Lucas, G. Wang, et al., Trends in electrocatalysis on extended and nanoscale Pt-bimetallic alloy surfaces, Nat. Mater. 6 (2007) 241–247, https://doi.org/10.1038/nmat1840.

[24] K.A. Stoerzinger, W.S. Choi, H. Jeen, H.N. Lee, Y. Shao-Horn, Role of strain and conductivity in oxygen electrocatalysis on LaCoO3 thin films, J. Phys. Chem. Lett. 6 (3) (2015) 487–492, https://doi.org/10.1021/jz502692a. Epub 2015 Jan 22 PMID: 26261968.

[25] J.M. Gallardo, P. Gümpel, J. Strittmatter, Phase change behavior of nitinol shape memory alloys influence of heat and thermomechanical treatments, Adv. Eng. Mater. 4 (2002) 437–452.

[26] S.K. Patel, B. Swain, R. Roshan, N.K. Sahu, A. Behera, A brief review of shape memory effects and fabrication processes of NiTi shape memory alloys, Mater Today Proc, vol. 33, Elsevier Ltd, 2020, pp. 5552–5556. doi: 10.1016/j.matpr.2020.03.539.

[27] D.S. Ford, White sr. thermomechanical behavior of 55ni45ti nitinol, Acta Mater. 1996 (1996) 44.

[28] M. Du, L. Cui, Y. Cao, A.J. Bard, Mechanoelectrochemical catalysis of the effect of elastic strain on a platinum nanofilm for the orr exerted by a shape memory alloy substrate, J. Am. Chem. Soc. 137 (2015) 7397–7403, https://doi.org/10.1021/jacs.5b03034.

[29] P. Strasser, S. Koh, T. Anniyev, J. Greeley, K. More, C. Yu, et al., Lattice-strain control of the activity in dealloyed core-shell fuel cell catalysts, Nat. Chem. 2 (2010) 454–460, https://doi.org/10.1038/nchem.623.

[30] W. He, M. Han, P. Goudeau, B.E. Le, P.O. Renault, S. Wang, et al., Strain transfer through film-substrate interface and surface curvature evolution during a tensile test, Appl. Surf. Sci. 434 (2018) 771–780, https://doi.org/10.1016/j.apsusc.2017.09.164.

[31] J. Böhn, P. Gruber, R. Spolenk, A. Stierle, A. Wanner, E. Arzt, Tensile testing of ultrathin polycrystalline films: a synchrotron-based technique, Rev. Sci. Instrum. 75 (2004) 1110–1119, https://doi.org/10.1063/1.1669124.

[32] A.C. Pronk, Theory of the four point dynamic bending test part I: general theory, Road & Hydraulic Engineering Institute, Delft, 2006.

[33] A.R. Sandy, S.G.J. Mochrie, D.M. Zehner, K.G. Huang, D. Gibbs, Structure and phases of the Au(111) surface: X-ray-scattering measurements, Phys. Rev. B 43 (1991) 4667.

[34] M.A. Meyers, K.K. Chawla, K. Kumar, Mechanical behavior of materials, Cambridge University Press, 2010.

[35] A. Alobaid, C. Wang, R.A. Adomaitis, Mechanism and Kinetics of HER and OER on NiFe LDH Films in an Alkaline Electrolyte, J. Electrochem. Soc. 165 (2018) J3395–J3404, https://doi.org/10.1149/2.0481815jes.

[36] G. Abadias, I. Schuster, A. Marty, B. Gilles, Epitaxial-strain-stabilized ordering in $Au_{1-x}Ni_x$ alloy thin films grown by MBE-Ni- alloy thin films grown by MBE, Phys. Rev. B 61 (2000) 6495–6506, https://doi.org/10.1103/PhysRevB.61.6495.